

Use of atomic-force microscopy and of a parallel irradiation geometry for in-depth characterization of damage produced by swift Kr ions in silicon

L. P. Biró and J. Gyulai

KFKI-Research Institute for Materials Science, P.O. Box 49, H-1525 Budapest, Hungary

K. Havancsak

Institute for Solid State Physics of Eötvös University, Múzeum krt. 6-8, H-1088 Budapest, Hungary

A. Yu. Didyk

Joint Institute for Nuclear Research, 141980 Dubna, Russia

S. Bogen and L. Frey

Fraunhofer-Institut für Integrierte Schaltungen, IIS-B, Schottkystr.10, 91058 Erlangen, Germany

(Received 22 March 1996; revised manuscript received 24 June 1996)

Silicon samples were irradiated with 209 MeV Kr ions in a direction parallel with the (100) plane. The variation vs distance from the irradiated edge, the (010) plane, i.e., vs depth, of the defects produced by the irradiation was evaluated *without any sample preparation* by atomic-force microscopy (AFM) and spreading resistance measurement on the (100) plane. Both methods indicate a penetration depth of 28 μm , in good agreement with the value given by Monte Carlo (TRIM) range calculation. AFM measurements allowed distinction between four depth zones to which different damage production mechanisms can be ascribed. [S0163-1829(96)01838-3]

In recent years, continuous efforts have been undertaken for better understanding of the damage production by swift heavy ions. Most thoroughly investigated are oxides,¹ recently a theoretical description of latent track formation was given for magnetic insulators.² Another category of intensively studied materials are polymers, for which practical applications have been already achieved.³ Metals have been considered for a long time as not showing any track formation process. Track formation was found recently in alloys like NiZr₂ and NiTi (Ref. 4) at values of electronic stopping power, $(dE/dx)_e$, of more than 40 keV/nm. Even more recently, experimental evidence for tracks having been produced in Ti by 845 MeV Pb ions, and by 18 MeV C₆₀ ions,⁵ demonstrated that metals, also, are susceptible for track formation. Semiconductors, however, seem to have received less attention. Results on Si and Ge indicate that they have different damage accumulation mechanisms.⁶

In the case of insulators, the most frequently applied investigation techniques are chemical etching and transmission electron microscopy.³ Etching is inefficient to investigate the damage production itself, since the damaged regions are those that are dissolved first. Transmission electron microscopy (TEM) is very powerful but at the same time it implies very delicate sample preparation. For magnetic materials, methods like Mössbauer spectroscopy, based on the changes of bulk magnetic properties in and around the ion track have been used.² Variations in the electrical resistance of foils with thickness in the μm range,⁷ or of bulk samples,⁶ have been used to characterize damage production. On the basis of TEM results, it is generally accepted that the damaged regions have a cylindrical geometry. However, one should keep in mind that TEM, or high-resolution TEM even more, has a limited depth resolution. In most cases thus, the ex-

posed depth region is of the order of 100 nm, i.e., a small fraction of the track tens of microns in length. If one wants to study objects with nanometer dimensions, the size of the observation window is limited, too. Therefore, scanning tunneling microscopy (STM) and atomic-force microscopy (AFM) which are able to scan windows of several tens of μm and have at the same time a resolution in the vertical direction of the order of a nm (AFM) or of an Å (STM), offer advantages to study swift heavy ion tracks with extreme aspect ratios. AFM has been successfully applied to investigate the impact features of swift heavy ions on the surface of mica⁸ and of the layered superconductor 2H-NbSe₂.⁹ Recently, we reported STM results on graphite irradiated by 215 MeV Ne ions.¹⁰ The examination of the irradiated surface by these high-resolution surface bound methods is not able to yield *direct* information on the processes taking place in deeper regions of the sample. Therefore, in this paper an attempt is reported, to gain insight in the deeper lying processes by irradiating a cleaved, rectangularly shaped sample from the edge—(010) plane—and searching for modifications on its perpendicular surface—(100) plane—being *parallel with the incoming beam*. The irradiation geometry is showed schematically in Fig. 1. We will call the distance from the (010) edge the “depth.”

Silicon samples of approximately $1 \times 0.5 \text{ cm}^2$ were cleaved from a 4–6 $\Omega \text{ cm}$ *p*-type (100) Si wafer. The samples were irradiated by 209 MeV Kr with the beam parallel to the (100) plane polished by the manufacturer. Extreme care was taken to avoid contamination of any kind, as we wanted deliberately to avoid any surface treatment. This polished surface was used for tapping mode AFM (Nanoscope III) investigation and for spreading resistance (SR) measurement. Doses of 10^{12} cm^{-2} , and 10^{13} cm^{-2} were

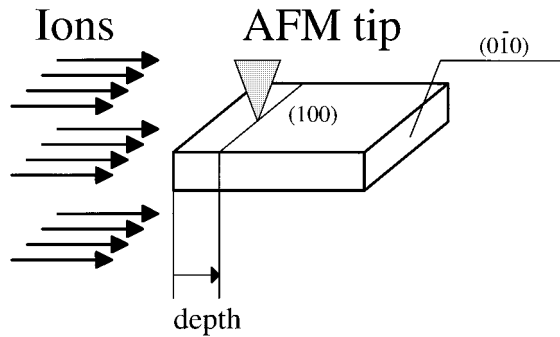


FIG. 1. Schematic presentation of the irradiation geometry used.

used. The measured root-mean-square (RMS) roughness of nonirradiated reference samples was in the range of 0.09 nm, a somewhat lower value than reported in Ref. 11.

Detailed investigation was carried out on the sample with a dose of 10^{12} ions cm^{-2} . First, the irradiated edge was located by scanning with a large scan size, so that the sample edge became visible on one side of the scanned window. Then, areas of $1 \times 1 \mu\text{m}^2$ were scanned and the offset value was increased so that the center of each new window was situated $1 \mu\text{m}$ deeper than that of the previous one. Crater-like features with characteristic depth and height in the nm range were found. In each image the RMS roughness value was calculated over the whole image (with all visible features included). For each image a reference RMS roughness value was taken from a square of $250 \times 250 \text{nm}^2$ which was placed in a way that it contained the smallest possible number of features (frequently, none). While the RMS roughness values in the $250 \times 250 \text{nm}^2$ squares varied in the range 0.1–0.15 nm in the first $18.5 \mu\text{m}$ from the edge, the roughness of the $1 \mu\text{m}^2$ areas vs depth showed minima and maxima due to distinctive features produced by the irradiation. The fact that the reference RMS roughness values (taken from the $250 \times 250 \text{nm}^2$ squares) remained around the value of 0.125 nm shows that the imaging conditions, and the tip status were not modified while the observation window center was moved in steps of $1 \mu\text{m}$. This is an indication that the minima and maxima observed are indeed due to the features produced by irradiation. In order to improve statistics without reducing depth resolution, an area of $1 \times 28 \mu\text{m}^2$ was also used. This larger area was moved in $1 \mu\text{m}$ steps through an image of $60 \times 60 \mu\text{m}^2$, and the corresponding RMS values were calculated. The results are shown in Fig. 2. Salient features of the two series of RMS measurements coincide satisfactorily, i.e., characteristic minima and maxima lie in the same depth. The shift about 0.5 nm between the two curves corresponding to the measurement area of $1 \times 1 \mu\text{m}^2$, and $1 \times 28 \mu\text{m}^2$, respectively, is produced by the apparent bending of the sample when the scan width is increased in a scanning system with a tube piezo. This effect is particularly strong when the lateral size of the scanned area, $28 \mu\text{m}$, is exceeding by several orders of magnitude the RMS roughness value of 0.1 nm.

To get further insight in the damage production process, spreading resistance¹² (SR) measurement was carried out in steps of $2.5 \mu\text{m}$ starting from the (010) edge. This method is based on measuring the resistance between two contacts which are pressed with a well defined load against the

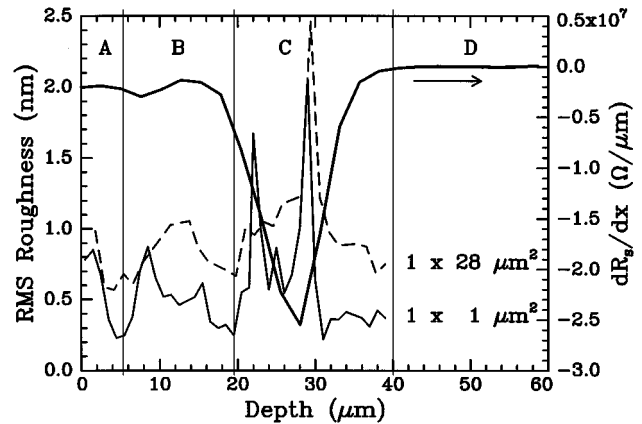


FIG. 2. Sample RMS roughness vs depth measured by AFM in areas of $1 \times 1 \mu\text{m}^2$, and in areas of $1 \times 28 \mu\text{m}^2$, moved in steps of $1 \mu\text{m}$ through a $60 \times 60 \mu\text{m}^2$ image. In addition the spatial derivative of spreading resistance R_s is given.

sample surface. We used a contact distance of $60 \mu\text{m}$, and a load of 10 g.

The SR values have a general trend of decreasing from the highest value of $2.92 \times 10^8 \Omega$, at $2.5 \mu\text{m}$ from the edge, to values around $1.1 \times 10^7 \Omega$ at $40 \mu\text{m}$ and deeper. Control measurements on not irradiated samples did not show significant variation of the SR values over the same depth range. For sake of clarity, the spatial derivative of the SR measured on the sample irradiated with a dose of 10^{12} Kr ions cm^{-2} , (dR_s/dx), was plotted in Fig. 2.

Four distinct zones can be identified in Fig. 2. The typical features of zone A, ranging from 0 to $5 \mu\text{m}$, are displayed in Fig. 3. For all AFM images shown here, the impinging ions enter from the right. The well-developed features are some-

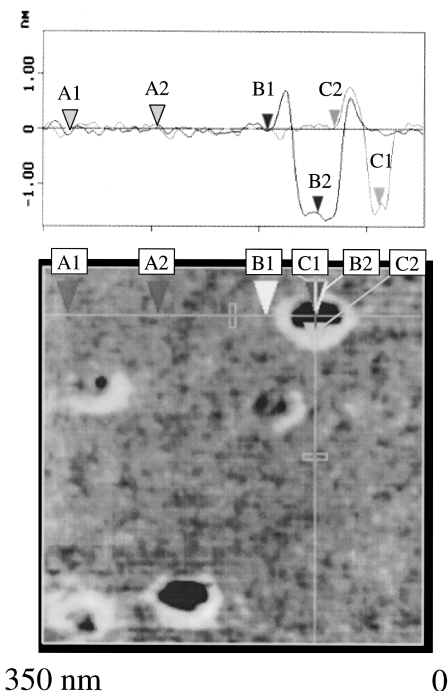


FIG. 3. AFM image of an area with typical craterlike features (type A), scan size $350 \times 350 \text{nm}^2$. The linear RMS roughness value along the line marked by A1 and A2 is 0.046 nm.

what elongated in the beam direction, with lengths ranging from 90–100 nm and the widths of 60–80 nm. Their depth is in the range of 1–1.5 nm. There are also less well developed features which also have an elongated shape. These appear similar to the previous features, but may be located further below the (100) surface. In region A, the maximum value of the RMS roughness is measured in the image centered by 1.5 μm from the edge. According to TRIM (Ref. 13) predictions, the value of electronic stopping, $S_e = (dE/dx)_e$ of 209 MeV Kr in silicon is $9.73 \times 10^3 \text{ keV}/\mu\text{m}$. The maximum value of S_e is at 180 MeV, $9.78 \times 10^3 \text{ keV}/\mu\text{m}$, expected at 3 μm from the edge. For samples irradiated with higher dose ($10^{13} \text{ ions}/\text{cm}^2$) a large number of elongated, partly overlapping holes was produced in zone A. As their number is around $70 \mu\text{m}^{-2}$, statistical evaluation was possible. For the image taken in the first micron, the histogram of length to width ratios is extended from 0.8 to 4, with the maximum at 1.5. Between 3 and 4 μm the histogram is extended between 0.8 and 2.8, with the maximum situated at 1. For both depth regions the average width is 52 nm. No features of this type were observed for depths greater than 5 μm . The statistical analysis shows that with increasing depth, the features tend to take a circular shape, and further on they vanish.

The type A features are attributed to damage produced by electronic stopping. The variation in their shape and number is in agreement with the damage morphology proposed by Toulemonde, Bouffard, and Studer¹ for $\text{Y}_3\text{Fe}_5\text{O}_{12}$. According to their work, there is a threshold value of S_e under which no track production is registered. As S_e increases over the threshold, single damage regions with spherical shape appear. With further increasing of S_e , the damage regions develop a more elongated shape, which finally will lead to continuous tracks. It must be pointed out, that the conditions in which the features were produced in our experiment (at the sample surface), may differ strongly from those in which ion tracks develop in the bulk. Having this observation in mind, and the shallow depths in the range of 1 nm, the type A features are attributed to explosive evaporation on the sample surface produced by ‘‘heating’’ due to electronic stopping effects. The radius of the cylinder of molten material for amorphous Si irradiated with swift heavy ions was calculated to be about of 0.5 nm for $S_e = 10^4 \text{ keV}/\mu\text{m}$.¹⁴ The significantly higher extension (short axis) of the type A features is attributed to a slower dissipation of heat at the sample surface facing the vacuum.

The typical features for region B, ranging from 5 to 18.5 μm , are shown in Fig. 4. These are circular, and have a well-developed crater in the center with material piled up around the craters. Less developed features with similar characteristics can also be seen in these images. In the depth range around 10 μm , a clearly different type of structures—hills of 13–15 nm height and 80–100 nm in diameter—with a density of $2\text{--}3 \mu\text{m}^{-2}$ are found together with type B features with a density around $50 \mu\text{m}^{-2}$. The type B features are attributed to knocked-on Si atoms which move perpendicular to the direction of the incoming ion. How well the structure is developed depends on the depth at which the collision generating the knocked-on Si took place. According to TRIM simulation, in the depth region from 4 to 8 μm , 6.6% of the incoming ions will generate secondary cascades extended over 300 nm. Taking into account that only half of

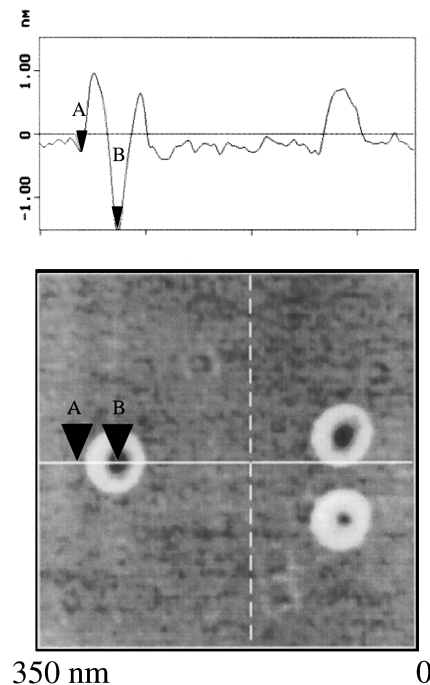


FIG. 4. AFM image of area with type B features, scan size $350 \times 350 \text{ nm}^2$. The continuous white line was moved along the broken white line to find the diagonal section. Note the less visible features with similar structure in the upper left-hand and lower right-hand quarter of the image.

secondary cascades is directed towards the surface, and that whether the secondary cascade reaches the surface or not, depends on the angle between the surface and the trajectory of the secondary cascade, from TRIM simulation one can expect $46 \text{ features } \mu\text{m}^{-2}$. At a depth of 16 μm the energy of Kr ions has dropped to around 50 MeV, about to one third of the value of 169 MeV at 4 μm . This means that although the number of knocked-on Si atoms may increase, the lateral range of those responsible for B-type features decreases, thus most of them will not reach the surface.

In agreement with the RMS roughness values, the SR measurement shows that dR_s/dx increases from 6 to 13 μm , i.e., the production of extended lateral subcascades is confirmed by the resistance variation vs depth. Region C, ranging from 18.5 to 40 μm , is the region around the projected range R_p . As in this region it was barely possible to find a square of $250 \times 250 \text{ nm}^2$ without features produced by the irradiation, the RMS roughness values measured in this area deviate from the value of 0.1 nm to values as high as 0.3 nm. The region is characterized by a large number of overlapping craterlike features and some large hills with characteristics similar to those observed in region B. While the small craters are a result of the knocked-on Si atoms leaving the target, it is possible that the large hills are produced by those Kr ions which have been deviated to a trajectory pointing towards the surface. A typical image is shown in Fig. 5, centered at a depth of 28 μm , i.e., at a depth at which the RMS roughness values reach the maximum and the strongest variation of resistance vs depth is found. According to the TRIM code, an R_p value of 27 μm is expected for 209 MeV Kr ions in silicon.

Beyond 40 μm the measured resistance values are around

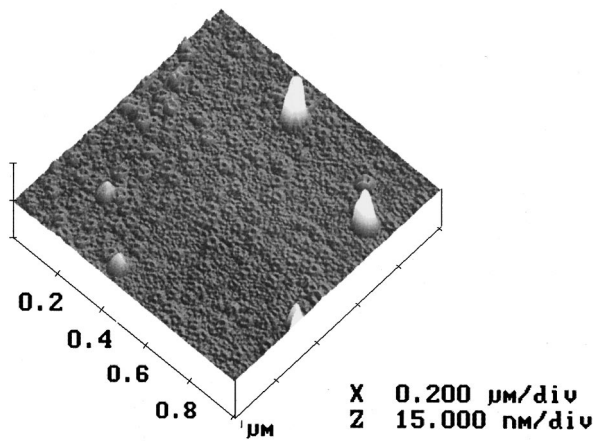


FIG. 5. AFM image centered at a depth of $28 \mu\text{m}$ in three-dimensional presentation. Note the overlapping craters and large hills of 15 nm height.

$1.1 \times 10^7 \Omega$. In this region D , a lower density of small craters like those in region C is still present. They are attributed to the channeled fraction of the beam, which has a higher penetration depth.

It should be noted that although the irradiation was carried out approximately in channeling direction, the most significant change in resistance is at R_p given by the TRIM code, which does not account for channeling. The use of the irradiation geometry for AFM and SR samples proved to be a valuable tool in monitoring damage vs depth for samples irradiated with swift heavy ions. The most important advantages are that (i) no sample preparation is needed, thus artifacts that could be produced, during grinding, sputtering, etc., can be excluded; (ii) the whole depth range is accessible for measurements on the same sample; (iii) the examination of large areas as compared with characteristic track dimensions allow statistical evaluation. In future experiments, lower irradiation doses will be used to investigate the history of single ion tracks throughout the entire range.

We are indebted to Professor H. Ryssel for making it possible for the AFM work to be carried out, and for H. Kotouc for the spreading resistance measurements. The work was partly supported by OTKA Grant No. T017344 in Hungary and L.P.B. gratefully acknowledges the Eötvös Hungarian State Fellowship Committee for financial support.

¹M. Toulemonde, S. Bouffard, and F. Studer, Nucl. Instrum. Methods Phys. Res. Sect. B **91**, 108 (1994).

²G. Szenes, Phys. Rev. B **51**, 8026 (1995).

³Reimar Spohr, *Ion Tracks and Microtechnology* (Vieweg, Braunschweig, 1990), p. 224.

⁴A. Dunlop, D. Lesueur, and A. Barbu, J. Nucl. Mater. **205**, 426 (1993).

⁵H. Damak, A. Dunlop, and D. Lesueur, Phys. Rev. Lett. **74**, 1135 (1995).

⁶M. Levalois, P. Bogdanski, and M. Toulemonde, Nucl. Instrum. Methods Phys. Res. Sect. B **63**, 14 (1992).

⁷A. Dunlop, D. Lesueur, P. Legrand, and H. Damak, Nucl. Instrum. Methods Phys. Res. Sect. B **90**, 330 (1994).

⁸F. Thibadau, J. Cousty, E. Balanzat, and S. Bouffard, Phys. Rev. Lett. **67**, 1582 (1991).

⁹P. Bauer, C. Giethmann, M. Kraus, T. Marek, J. Burger, G. Kre-

iselmeyer, G. Saemann-Ischenko, and M. Skibowski, Europhys. Lett. **23**, 585 (1993).

¹⁰L. P. Biró, J. Gyulai, and K. Havancsak, Phys. Rev. B **52**, 2047 (1995).

¹¹M. Yasutake, S. Wakiyama, and Y. Kato, J. Vac. Sci. Technol. B **12**, 1572 (1994).

¹²For details on the SR method, see for example, H. Ryssel and I. Ruge, *Ion Implantation* (Wiley, Chichester, 1986), p. 193, and references therein.

¹³J. Biersack and L. Haggmark, Nucl. Instrum. Methods **174**, 257 (1980); J. F. Ziegler, J. P. Biersack, and U. Littmark, *The Stopping and Ranges of Ions in Solids* (Pergamon, New York, 1985), Vol. 1.

¹⁴M. Toulemonde, C. Dufour, and E. Paumier, Phys. Rev. B **46**, 14 362 (1992).